PCCP

View Online
Dynamic Article Links

Cite this: DOI: 10.1039/c1cp22428j

www.rsc.org/pccp

PAPER

Resonant IR multi-photon dissociation spectroscopy of a trapped and sympathetically cooled biomolecular ion species

Ch. Wellers,† A. Borodin,*† S. Vasilyev, D. Offenberg and S. Schiller

Received 27th July 2011, Accepted 20th September 2011
DOI: 10.1039/c1cp22428j

In this work we demonstrate vibrational spectroscopy of polyatomic ions that are trapped and sympathetically cooled by laser-cooled atomic ions. We use the protonated dipeptide tyrosine–alanine ($HTyrAla^+$) as a model system, cooled by barium ions to less than 800 mK secular temperature. The spectroscopy is performed on the fundamental vibrational transition of a local vibrational mode at 2.74 μm using a continuous-wave optical parametric oscillator (OPO). Resonant IR multi-photon dissociation spectroscopy (R-IRMPD) (without the use of a UV laser) generates charged molecular fragments, which are sympathetically cooled and trapped, and subsequently released from the trap and counted. We measured the cross section for R-IRMPD under conditions of low intensity, and found it to be approximately two orders smaller than the vibrational excitation cross section. The observed rotational bandwidth of the vibrational transition is larger than the one expected from the combined effects of 300 K black-body temperature, conformer-dependent line shifts, and intermolecular vibrational relaxation broadening (J. Stearns *et al.*, *J. Chem. Phys.*, 2007, **127**, 154322–154327). This indicates that as the internal energy of the molecule grows, an increase of the rotational temperature of the molecular ions well above room temperature (up to on the order of 1000 K), and/or an appreciable shift of the vibrational transition frequency (approx. 6–8 cm^{-1}) occurs.

1 Introduction

In the field of cold, trapped molecules, one topic under current study is the development and refinement of suitable spectroscopic methods. Concerning more specifically translationally cold molecular ions, often produced *via* sympathetic cooling by laser-cooled ions, a few studies have been performed recently, on diatomic molecular ions. Ro-vibrational spectroscopy is one example, applied in particular to HD^+ and MgH^+. Fundamental ($\Delta v = 1$),[1–4] first ($\Delta v = 2$),[1] and third overtone ($\Delta v = 4$)[5,6] vibrational spectroscopy, with resolution of the rotational structure, has been described. In the simplest case, the spectroscopy consisted in a simple variant of resonance-enhanced multiphoton dissociation (1 + 1′ REMPD), where a vibrational transition is driven by one photon and a second, UV photon dissociates the molecule by exciting it from the vibrationally excited level to a non-binding electronically excited state. The reduction of the number of intact molecular ions is then detected in an appropriate way. More recently, in our group we have also employed 1 + 1′ + 1″ REMPD on HD^+, where the first photon performed a rotational or vibrational excitation, followed by a vibrational excitation and then dissociation by a UV photon.[7] It is of interest to explore if and how spectroscopy can be extended to sympathetically cooled molecular ions other than diatomic ones.

This work is devoted to a first methodological study of vibrational spectroscopy of a sympathetically cooled polyatomic molecular ion. Vibrational spectroscopy of complex molecular ions is a very important method for gaining information on structures of molecules, including biomolecules (see, *e.g.* ref. 8 and references therein), and for studying the energetics of fragmentation.[9] Apart from implementing vibrational spectroscopy, we investigate the question whether the rotational degrees of freedom of the molecules couple, *via* the ion–ion collisions between the molecules and other ions in the trap, to the translational ones, which are sympathetically cooled to less than 800 mK (secular motional temperature). The molecular ion species used, protonated tyrosine–alanine ($HTyrAla^+$), is a test case appropriate for the present purposes since a previous study by Stearns *et al.*[10] has shown that it exhibits a spectrally narrow vibrational transition. The vibrational linewidth observed in that work included the width of the rotational band, whose details were unresolved, due to experimental reasons, but also because of the small rotational constant exhibited by this relatively large molecule.

We found in the course of our studies that resonant IR multi-photon dissociation (R-IRMPD) can be applied to sympathetically cooled $HTyrAla^+$ ion ensembles. Here, only

Institut für Experimentalphysik,
Heinrich-Heine-Universität Düsseldorf, 40225 Düsseldorf, Germany.
E-mail: andrii.borodin@uni-duesseldorf.de
† First authorship shared.

photons of energy resonant with a vibrational transition of a specific vibrational mode are used. Upon absorption of the photon, the vibrational energy is distributed on a time scale of less than a nanosecond[11] to other internal degrees of freedom, by intramolecular vibrational relaxation (IVR). After that, another photon of the same energy can be absorbed on the same transition.[12,13,14] (This is not possible with sympathetically cooled diatomic ions, since there are no other internal degrees of freedom, nor sufficient collisional vibrational relaxation because UHV conditions are maintained.) The photon absorption process is repeated, allowing the molecule to collect internal energy until it will be large enough to break certain molecular bonds, leading to generation of charged fragments, and a reduction in the number of parent molecules. This technique is used in spectroscopy of trapped complex molecular ions, but has so far been applied only to uncooled molecules, to our knowledge. It is used in conjunction with large-scale, pulsed infrared laser systems, *e.g.* free-electron lasers, which allow a very wide spectral coverage[8,15] and therefore a rather complete study of the vibrational spectrum. For other methods of spectroscopy of polyatomic molecular ions, using buffer gas cooling, see *e.g.* ref. 32.

The present laboratory experiment is an example that such studies are becoming possible with laboratory laser sources only, even continuous-wave ones. Indeed the IR spectral coverage with cw sources such as OPOs, quantum cascade lasers and difference frequency generators[16] is rapidly increasing.

2 Experimental apparatus

In this work, a previously developed, general-purpose apparatus for sympathetic cooling of a large variety of complex molecular ions is employed.[17] Fig. 1 shows an overview of the apparatus. The molecular ions travel from left, the ion source, to the right, the ion trap. Mass-to-charge selected molecular ions are trapped in the ion trap and are sympathetically cooled *via* Coulomb interaction with a laser-cooled atomic ion ensemble species. Depending on their mass and charge, polyatomic ions can be cooled to translational temperatures well below 1 K.[20] The long storage time of few tens of minutes combined with the well-defined and nearly collisionless environment in the ion trap provides very particular conditions for spectroscopy.

As the electrospray ionization takes place at atmospheric pressure, while the achievement of sub-Kelvin temperature using laser cooling requires ultra-high vacuum conditions, high demands are made on the vacuum system. Both conditions are fulfilled using a differentially pumped vacuum setup that provides a pressure gradient of more than 13 orders of magnitude, sustained by in total 11 vacuum pumps.

The molecular ion source is a modified commercial mass spectrometer Finnigan SSQ 700, based on electrospray ionization (ESI). A large variety of neutral molecules can be protonated (*i.e.* one or more proton(s) attach(es) to the neutral molecule by polarization interaction) in the ESI molecular ion source,

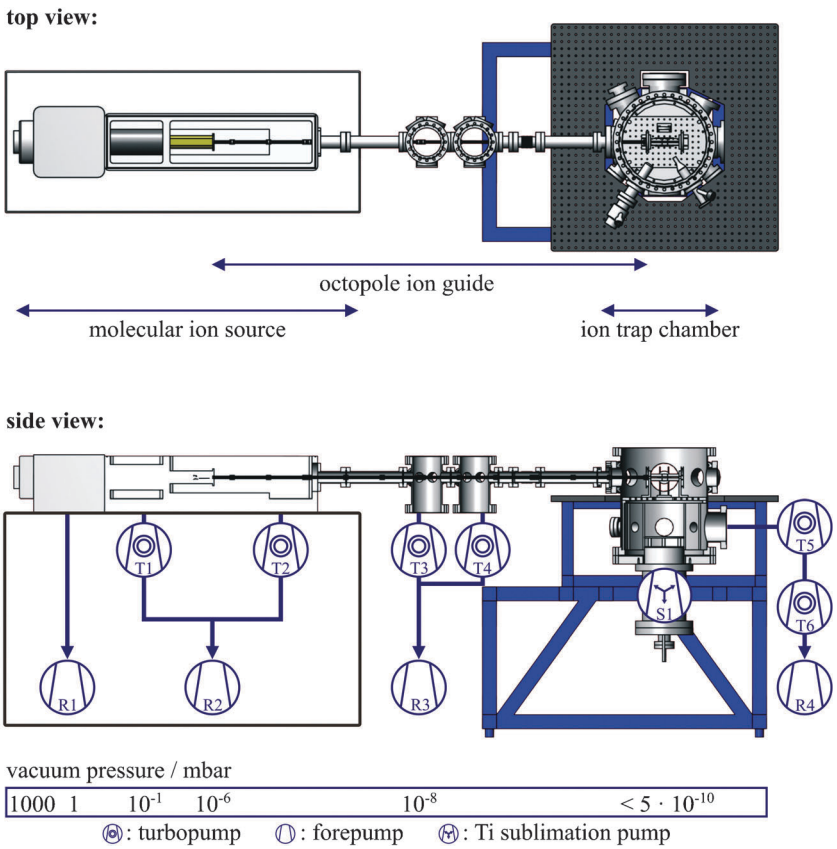

Fig. 1 Overview of the vacuum setup. Top and side views of the vacuum setup consisting of the electrospray ionization (ESI) molecular ion source, the octopole ion guide, and the ion trap vacuum chamber in which the molecular ions are trapped, cooled and manipulated in a linear quadrupole ion trap. The vacuum pressure in the differential vacuum setup decreases from atmospheric pressure at the molecular ion source inlet (where a solution is fed into the ion source) to ultra-high vacuum values in the ion trap chamber.[18,19]

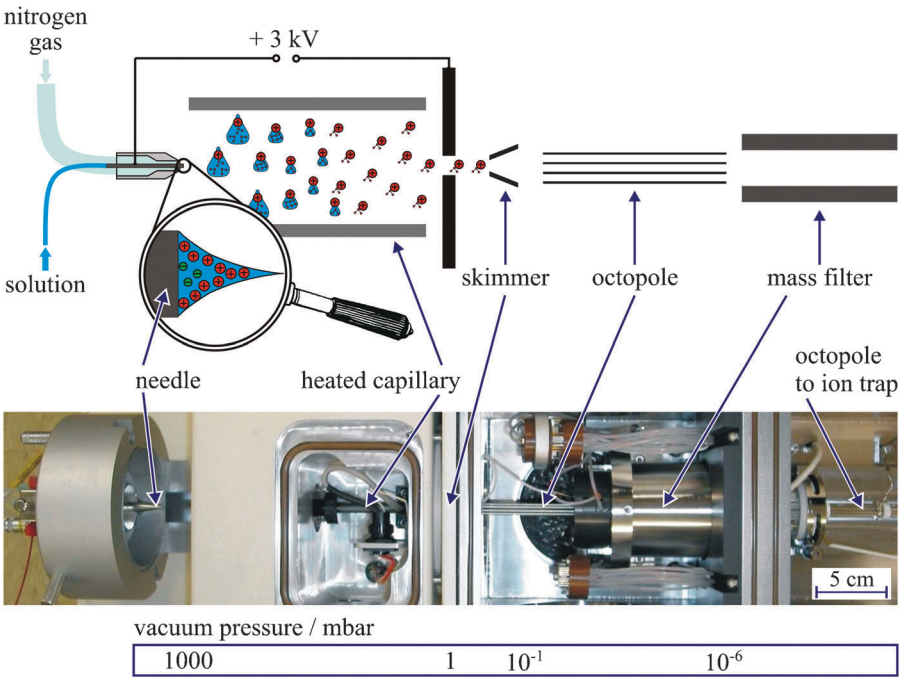

Fig. 2 Principle and setup of the molecular ion source. The upper schematic diagram (not to scale) illustrates the principle of electrospray ionization as described in the text. The lower photo shows the uncovered molecular ion source, with the needle through which the solution with the molecular ions is sprayed, the heated capillary in which the solvent evaporates, the skimmer (covered by housing components) which serves as aperture, a short octopole used as ion guide, the quadrupole mass filter for selection of the ion species to be transferred to the ion trap, and the beginning of the 2 m long octopole which transfers the molecular ions to the ion trap. The pressures given below the photograph are approximate values for the atmospheric pressure region (1000 mbar), the skimmer region (1 mbar), the octopole region (10^{-1} mbar), and the following high vacuum region (10^{-6} mbar).

including molecules with masses exceeding 10 000 atomic mass units (amu). As Fig. 2 shows, the molecular ions are produced from a solution, which is sprayed as droplets into a vacuum chamber, where the solvent is evaporated until individual protonated molecular ions remain.

In the present study, a solution of 70 pmol l^{-1} dipeptide tyrosine–alanine in a solution of methanol + water (1 : 1 relative concentration) + 0.1% formic acid is prepared, in which protonated tyrosine–alanine forms ($HTyrAla^+$, mass 251 amu). The protons are supplied by the formic acid. The solution is filled into a syringe, from which it is sprayed at atmospheric pressure (1000 mbar) through a thin metal needle to which a positive high voltage is applied. The emerging solution is shaped by a streaming nitrogen gas into a so-called Taylor cone. Solution droplets break away from the Taylor cone and are accelerated towards a heated capillary (200 °C). The solvent evaporates and the droplets shrink until a critical size, known as Rayleigh stability limit, is reached. The droplets then break apart into smaller ones until bare molecular ions remain. The stream of molecular ions is transferred through the skimmer region at 1 mbar to the quadrupole mass filter with a short octopole ion guide. This mass filter is placed in the high-vacuum section of the apparatus, at about 10^{-6} mbar pressure. The quadrupole mass filter parameters are controlled by a computer, allowing purification of the ion stream and delivery of a species with a particular mass-to-charge ratio to the following apparatus section. After the mass filter, the molecular ions are coupled into a 2 m long radio frequency octopole ion guide which transfers the ions to the linear quadrupole ion trap placed in a cylindrical vacuum chamber at $<10^{-9}$ mbar, shown in Fig. 3. Details about the octopole guide can be found in ref. 18 and 21.

The RF trap consists of four cylindrical stainless steel rods with a diameter of 10 mm, which are divided into the middle electrodes of 20 mm length and the two endcap electrodes of 30 mm length. The smallest distance of the electrode surface to the trap axis is $r_0 = 4.36$ mm. With this geometry, the axial electric potential of the trap,[22,23]

$$\Phi_z = \kappa U_{EC} z^2,$$

has the coefficient $\kappa = 1500\ m^{-2}$. The RF voltages for radial ion confinement are applied to the middle and the endcap electrodes with an RF frequency of $\Omega = 2\pi \times 2.5$ MHz and a maximum amplitude of $U_{RF,max} = 500$ V. dc voltages of −20 to +20 V can be individually applied to the four middle electrodes to compensate external electric fields for exact symmetrization of the quadrupole field. Typical operation parameters are 200 V $< U_{RF} <$ 500 V and 5 V $< U_{EC} <$ 7 V.

The magnetic field that is necessary for laser cooling of $^{138}Ba^+$ ions is produced by two coils centered around the trap axis and mounted beyond the endcap electrodes (see Fig. 4). The coils produce a magnetic field in the trap center which is parallel to the trap axis and has a strength of approximately 5 G.

To count the trapped ions, they are released from the trap and led to a channel electron multiplier (CEM) mounted below the trap, serving as an ion detector (Fig. 4). When the

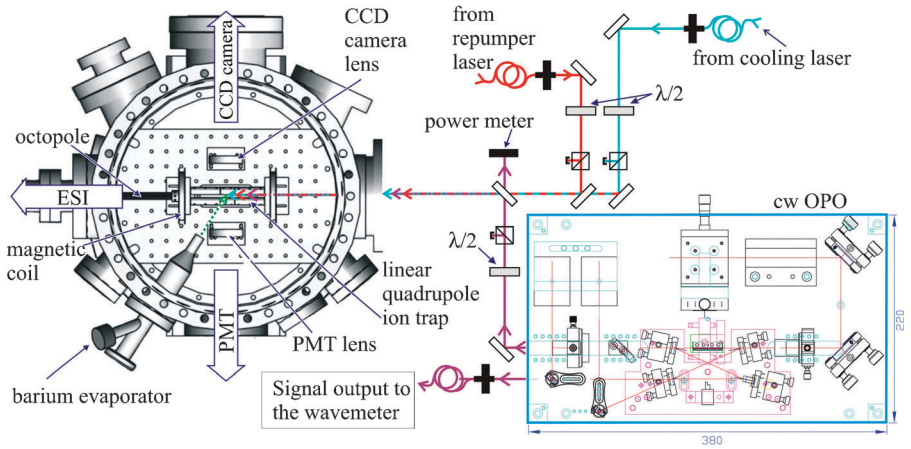

Fig. 3 Overview of the ion trap vacuum chamber. Molecular ions from the ESI ion source are transferred to the linear quadrupole ion trap *via* the octopole ion guide. The barium ions are produced with an ultra-high-vacuum suitable evaporator directed to the trap center (dashed green arrow). Cooling (493 nm), repumping (650 nm) and vibrational spectroscopy laser light (2.7 μm) (blue, red and violet arrows, respectively) enter the vacuum chamber through an axial sapphire viewport. The fluorescence light emitted by the laser-cooled $^{138}Ba^{+}$ ions is collimated by radially arranged lenses to direct it through glass viewports to a CCD camera and a photomultiplier (PMT), both located outside the vacuum chamber.[18] The dimensions of the OPO base plate are in mm.

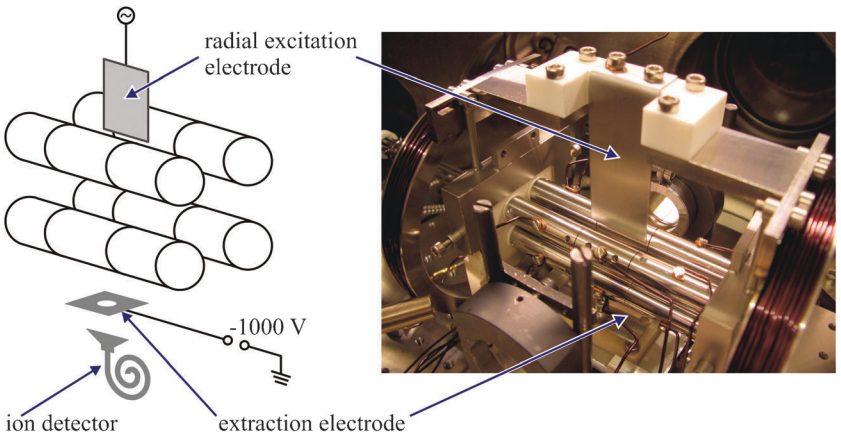

Fig. 4 Trap setup with cleaning and detection components. With an ac voltage scan applied to the radial excitation electrode, molecules with a specified mass-to-charge ratio can be removed from the trap. The identification of the stored ion species is *via* their mass-to-charge ratio, and is obtained *via* a controlled decrease of the ion trap RF amplitude and a simultaneous detection of the escaping ions. Detection is achieved by directing the ions by an extraction electrode to an ion detector mounted below the trap.

trap RF voltage U_{RF} is decreased, ions of mass m and charge q are not stably trapped any more once the value reaches

$$U_{RF}^{ex} = ar_0^2\Omega\sqrt{2\kappa U_{EC}\frac{m}{q}}.$$

Here a is a numerical factor describing the influence of the electric field of the extraction electrode. This simple expression holds in the limit of a single trapped ion and zero kinetic energy.

The escaping ions will be accelerated by an extraction electrode at a dc voltage of about −1000 V and counted. The number of detected ions *versus* the RF voltage represents a mass spectrum of the trapped ion ensembles ($q = e$ is assumed for all ions, as we have no evidence for higher charge states having been produced, trapped and sympathetically cooled). In the spectra shown below, the largest detectable mass (850 amu) corresponds to the RF amplitude used for normal trapping operation, $U_{RF}^{ex} = U_{RF} = 300$ V. By comparing the ion number detected by the counter with the number of ions initially contained in the Coulomb crystals (this number is obtained by Molecular Dynamic (MD) simulations on the basis of CCD images), we found that the ion detection efficiency is between 10 and 20%.

For the laser cooling of $^{138}Ba^{+}$ ions, a cooling laser at 493 nm (generated by sum-frequency mixing of a 920 nm diode laser wave and a 1064 nm Nd:YAG laser wave) and a repumper diode laser at 650 nm are required. Both cooling and repumping laser frequencies are locked to transfer cavities, which, in turn, are locked to the Nd:YAG laser, itself stabilized to a ro-vibrational transition of molecular iodine *via* Doppler-free saturation spectroscopy.

3 Preparation, cooling and analysis of ion ensembles

First, a barium ion crystal is prepared in the trap by an electron gun bombarding and ionizing metallic barium (ref. 24, Fig. 5(a)).

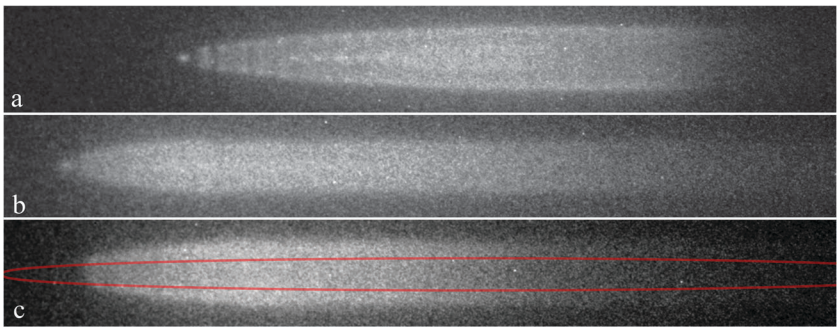

Fig. 5 Experimental CCD images of ion crystals. (a) A barium ion crystal, containing laser-cooled $^{138}Ba^+$ ions and sympathetically cooled ions of other Ba isotopes. The relative abundance of $^{138}Ba^+$ is 72%. The cooling laser's light pressure acts only on $^{138}Ba^+$, not on sympathetically cooled barium isotopes. The laser cooled ions are therefore pushed to the left with respect to the other isotopes, which are located on the right, in the dark region. Molecular impurity ions (BaO^+, $CO_2{}^+$) have been previously removed. (b) A crystal, radially compressed and axially prolonged by the (non-fluorescing) surrounding sympathetically cooled $HTyrAla^+$ ions. (c) The crystal after partial photodissociation of $HTyrAla^+$ ions by R-IRMPD. Sympathetically cooled ionized molecular fragments lighter than Ba^+ ions are trapped close to the trap axis, forming a dark region in the center of the crystal (marked in red). Compare with Fig. 8.

Some of these ions react with residual H_2O gas molecules to produce barium oxide ions. The electron gun also ionizes residual CO_2 gas. These molecular ion species are also trapped in the ion trap. In order to load molecular ions delivered *via* the octopole ion guide, the dc potential of the entry endcap is decreased and the ion guide is activated for several seconds. In addition, room temperature helium buffer gas (at (4–6) $\times$ 10^{-6} mbar) is injected into the trap using a piezoelectric valve. This acts as a buffer gas, in which collisions with the molecular ions reduce their kinetic energy sufficiently for capture in the trap (Fig. 6). The ions in the crystal also collide with the He atoms, causing its melting. The continued action of the cooling laser leads to a steady state corresponding to a cold gas. After restoring the entry electrodes' potential the valve is closed and the pressure of the buffer gas decreases within several seconds due to pumping. Then the barium cloud crystallizes again and sympathetically cools the trapped molecular ions (Fig. 5(b)). For species-selective cleaning we apply a suitably strong ac electric field to a radial excitation electrode (see Fig. 4). It induces a radial secular motion of sufficiently large amplitude so that the resonant ions are ejected from the trap. The frequencies of the excitation are made to cover the secular resonance frequencies of undesired ions. The cleaning is used in particular to remove $CO_2{}^+$ and BaO^+.

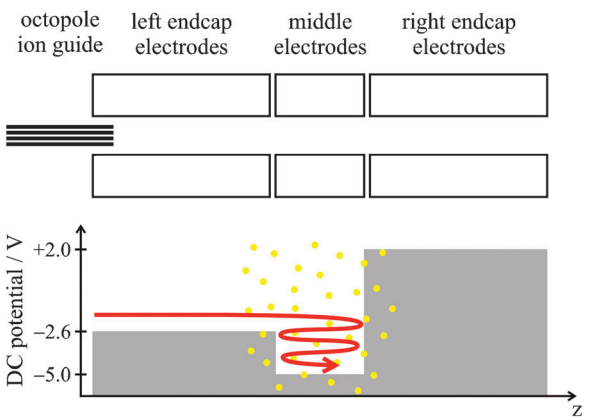

Fig. 6 Schematic principle of loading of the ion trap with molecular ions coming from the ion source. The dc potential of the left endcap electrodes is temporarily lowered, allowing entrance of the ions. Their kinetic energy (red arrow) is reduced by collisions with helium buffer gas (yellow dots), leading to trapping.

Two ion extraction spectra obtained as described in Section 2 are compared in Fig. 7(a) to show the significant influence of laser cooling and sympathetic cooling. The ensembles contained Ba^+, BaO^+ and $HTyrAla^+$ and had kinetic energies corresponding to room temperature (red), achieved by collisions with He buffer gas (lasers were off), and below 1 K (blue), achieved by laser cooling. In the 300 K case, the peaks in the extraction spectrum are broadened, indicating a larger distribution in the energy of the trapped ions. For the cooled ensemble, not only the peak of the laser-cooled Ba^+ ions is narrower, allowing us to resolve the peak of the sympathetically cooled BaO^+ ions, but also the one of $HTyrAla^+$. This latter peak narrowing is a qualitative proof of the sympathetic cooling of complex molecular ions.

The action of R-IRMPD on the ion ensemble is seen in Fig. 5(c), where a $Ba^+/HTyrAla^+$ ion crystal was exposed comparatively long to continuous-wave light at 2.74 μm. Fig. 7(b) shows the ion extraction spectra, which give detailed information about the contents of the ensemble. The $HTyrAla^+$ ions were nearly completely destroyed and fragments of different masses have appeared. For comparison, the red curve is the extraction spectrum of a crystal acquired directly after the preparation phase (no R-IRMPD), showing only the two ion species as expected (this spectrum is the same as the blue curve in Fig. 7(a)).

The information contained in the ion extraction spectrum together with the CCD images of the barium ions' fluorescence before and after extraction of the ions can be used to characterize the initial ion ensemble (initial numbers of ions of different species and their temperatures) and the final state (number of fragments and final temperature of different species).[20] MD simulations are performed for this purpose. Fig. 8 shows an example of the final state of an ensemble where R-IRMPD has partially photodissociated the $HTyrAla^+$ ions. A comparison with experimental CCD images reveals that the typical temperature of $HTyrAla^+$ is less than 800 mK. This value is

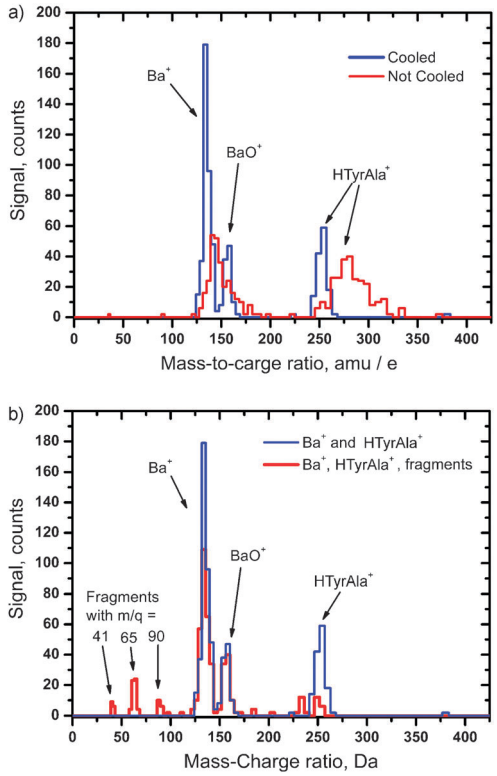

Fig. 7 (a) Mass spectrum of extracted ions, when the trapped ensemble was laser-cooled (blue) and buffer-gas cooled (300 K, red), respectively. The wider peaks in the 300 K case are due to the correspondingly larger kinetic energy distribution of the ions inside the trap. Note also that in the 300 K case, ions are extracted from the trap already at higher RF amplitudes as compared to cold ions. (b) Mass spectrum of a cold ion ensemble without R-IRMPD (blue) and with R-IRMPD (red).

the thermal energy associated with the secular motion. In addition, all ions perform micromotion. The micromotion energy of the $HTyrAla^+$ ions can be calculated from the trap parameters and the distance from the axis, and amounts to k_B (11.5 K) per ion.[25]

4 IR laser source

$HTyrAla^+$ molecular ions have a complex absorption spectrum, with many lines corresponding to fundamental and overtone excitation of local vibrational modes, complicated by the presence of a rotational structure.[10] The single line studied here is the fundamental vibration of the OH group bound to the phenol ring in the $HTyrAla^+$ dipeptide (Fig. 9). We used the idler wave of a continuous-wave OPO for the spectroscopy, since its high power and tunability provides experimental flexibility. The device is home-built, see Fig. 3.[16] It uses a ring cavity containing a periodically poled lithium niobate crystal, and is pumped by an independent Nd:YAG master laser (1064 nm), amplified by a fiber amplifier, with a maximum output of 9.5 W. Typically, 5 W are delivered *via* a fiber to pump the OPO ring cavity located next to the UHV chamber (Fig. 3). This OPO is tunable over a wide spectral range (2500–3000 nm) by changing the temperature of the nonlinear crystal. The typical output spectral linewidth is a few ten kHz, the output power is up to 2.5 W for the idler wave and up to 3 W for the signal wave (at the highest pump power). In order to prevent mode-hops, the OPO is stabilized using back reflections from the gratings in the crystal. The output wavelength of the idler radiation is determined by measuring the wavelength of the signal radiation, which is sent to a high-resolution wavemeter. The master laser is intrinsically frequency-stable on the time scale of interest here, its wavelength being 1064.49 nm. The idler wave of the OPO is sent into the trap axially, by an uncoated CaF_2 beam sampler. The power is adjusted by a combination of a polarizer and a rotated $\lambda/2$ wave retarding plate. The diameter of the idler beam inside the trap was measured as 0.86 mm.

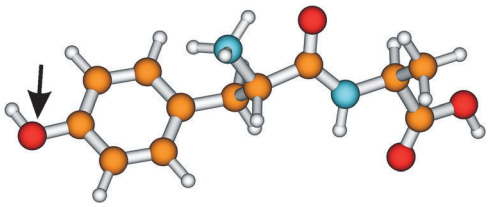

Fig. 9 3D view of the structure of $HTyrAla^+$ (conformer A). Atoms: carbon (orange), oxygen (red), nitrogen (blue) and hydrogen (white). The arrow indicates the phenol OH group in which the vibrational excitation studied here takes place.

5 Calibration

The molecular ion flux from the ESI source is not stable, showing both short-time fluctuation and longer-term trends, the overall flux variation being on the order of 25%. As a consequence, the number of trapped $HTyrAla^+$ ions varied from one loading to the next. In order to characterize the

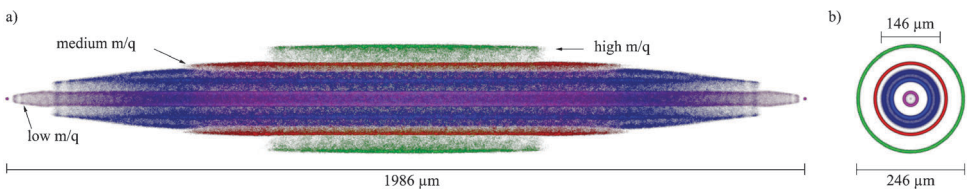

Fig. 8 Radial mass separation in a multi-species Coulomb crystal. Simulated images for the experimental trap parameters of a Coulomb crystal containing 440 molecular fragments (pink, mass 65 amu), 1190 Ba^+ ions (blue, all isotopes), 460 BaO^+ ions (red, 154 amu), and 230 $HTyrAla^+$ ions (green, 251 amu). The image shows the crystal as it would appear if all ions were fluorescing. In this simulation the cooling laser radiation pressure force is not taken into account. Compare to the experimental CCD images in Fig. 5, where only $^{138}Ba^+$ ions fluoresce and the radiation pressure force acts. (a) Side view. (b) Cross sectional view. Ions of lower mass arrange close to the trap axis, heavier ions arrange in shells around the lighter ions.

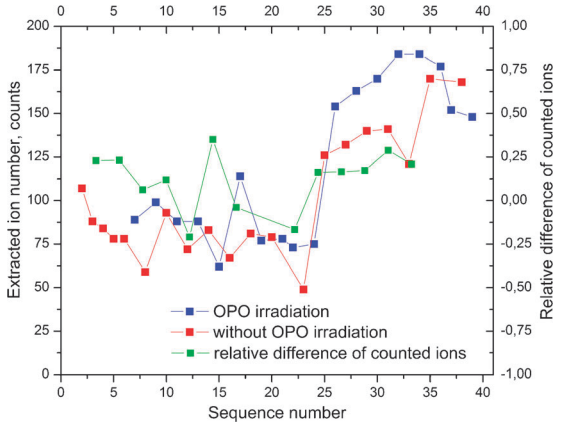

Fig. 10 Ion flux check and ion number conservation. Red: counts of extracted $HTyrAla^+$ without OPO irradiation. Blue: total counts of extracted $HTyrAla^+$ and its fragments. Green: relative difference of counted ions (right ordinate). The comparison of the two cases shows that the total count is equivalent to the number of loaded $HTyrAla^+$.

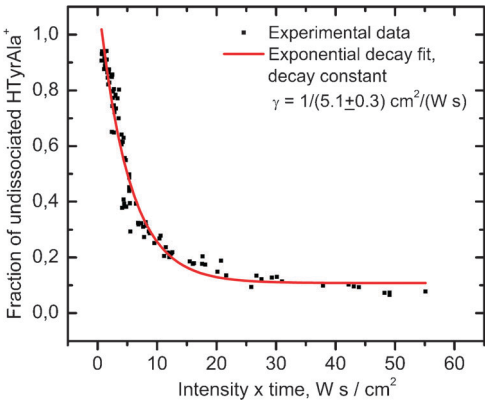

Fig. 11 Fraction of undissociated uncooled $HTyrAla^+$ ions as a function of irradiated energy. In this series of experiments, only $HTyrAla^+$ ions were trapped and cooled by 300 K He buffer gas, and irradiated for different times and at different OPO power levels. As the measurements were done on uncooled ions, significant broadening of the extraction spectra occurs (see Fig. 7). This limits the resolution of this method and gives rise to an additive noise. Therefore, a fit function with an offset has been used to model the data.

variations, the extraction spectra were recorded during a series of repeated $HTyrAla^+$ loadings without Ba^+. Interleaved procedures were used, alternating between OPO irradiation on and off. Also, the OPO power and its idler wavelength were changed within a wide range. Fig. 10 shows the measurements, taken over the course of 20 min. Here, the barium ion crystal remained the same, laser cooling was always on. The red points show the variation of the number of counts of extracted $HTyrAla^+$ ions. For comparison, the blue points show the interleaved measurements where after loading and buffer gas cooling, the $HTyrAla^+$ was partially photodissociated. Here, the number of counts of the fragments and of the undissociated $HTyrAla^+$ in the mass spectrum was added. The relative deviation (green) of this total number with respect to the average number of $HTyrAla^+$ detected in the previous and subsequent loadings is moderate, less than 25%. Thus, this total number of counts is used as a measure of the initial number of $HTyrAla^+$ after loading, which is not measurable in a nondestructive way, and also determines the effect of a spectroscopic excitation in terms of the relative photodissociation efficiency of the initial (parent) $HTyrAla^+$ ions. This procedure is quite useful, and more practical than extracting the initial number from MD simulations, which would be very time-consuming.

The typical ion extraction spectrum in Fig. 7 shows an advantage of having sympathetically cooled ions rather than uncooled ions: this method allows a quantitative characterization of the fragment ions. It is seen that there are at least three different types of products of photodissociation, having mass/charge ratios 41, 65 and 90 amu/e. Fragments with atomic mass close to $\frac{m}{q} = 138$ amu/e are hard to distinguish from $^{138}Ba^+$. We assume that there is no fragment with this mass which is proved by experiments with room-temperature ions.

A series of R-IRMPD experiments was made for room-temperature and sympathetically cooled ions, for different Coulomb crystal sizes and numbers of $HTyrAla^+$ ions trapped, for different OPO wavelengths, irradiation times and OPO powers. The extraction spectra were sorted into groups corresponding to different power ranges, OPO frequencies and irradiation times.

6 Results and discussion

Fig. 11 shows the fraction of undissociated $HTyrAla^+$ ions as a function of irradiated energy, given by the product of power and irradiation time, normalized to the beam cross sectional area. In this series of experiments, only $HTyrAla^+$ ions were trapped (in the presence of He buffer gas), irradiated for different times and powers (at the fixed bean diameter), while the OPO wavelength was close to the central wavelength of the observed spectrum. The fraction decreases exponentially with irradiated energy, indicating that a linear process is occurring, where a one-photon process dominates. Note that the dissociation rate is very small. At a typical power of 10 mW and the beam cross section used here, it is 0.34 s^{-1}, much smaller than spontaneous or IVR rate (see below). Taking into account the beam cross section and correcting for the non-uniform intensity distribution of the Gaussian OPO beam, we can deduce a (peak) R-IRMPD dissociation cross section of at least $\sigma_{diss,min} = 1.5 \times 10^{-20}$ cm^2 under our conditions. As the buffer gas ion cloud may have had a larger diameter than the laser beam, thus reducing the effective intensity experienced by the ions, this value is a lower limit. On sympathetically cooled ions, which are all located within the OPO wave, only a few measurements of dissociation as a function of irradiation time were performed at low intensity. The obtained decay constant is consistent with that given in Fig. 11, within the errors. Thus, σ_{diss} is similar to $\sigma_{diss,min}$.

As phenol is that part of $HTyrAla^+$ that carries the OH group excited by R-IRMPD, we can compare σ_{diss} with the peak absorption cross section deduced from a measurement of the same mode on phenol molecules, $\sigma_{PhOH,abs} = 7.4 \times 10^{-19}$ cm^2.[26] Here we have used the experimental oscillator strength value $f = 7.9 \times 10^{-6}$, and assumed a Lorentzian band shape with a FWHM of 6 cm^{-1}, obtained from a rotational band simulation at 300 K (see below). We can also consider the theoretical absorption cross section for our particular vibrational transition, obtained from the transition dipole moment of the mode as

Table 1 Low-energy conformers of $HTyrAla^+$: theoretical and experimental properties from ref. 10. The transition dipole moment components are given in the principal axis system. The experimental spectrum of ref. 10 was taken in steps of 0.5 cm^{-1}, thus the differences between the conformers' frequencies are only known with this resolution. The linewidth values are approximate. The observed vibrational frequency has a systematic uncertainty of 2 cm^{-1}. The theoretical vibrational frequencies were obtained from quantum chemical computations and corrected by a factor 0.954 in order to take into account anharmonicities of hydride frequencies. This factor has previously given a good fit for protonated amino acids

	Theoretical						Experimental	
				Rotational constants/GHz				
Conformer	Energy rel. to ground [kJ mol^{-1} = k_B (121 K)]	Vibr. freq. of PhOH mode/cm^{-1}	Transition dipole moment (d_x, d_y, d_z) [0.0104 D]	A	B	C	Vibr. freq./cm^{-1}	Line-width/cm^{-1}
A	0	3641.2	(9.96, 2.42, 3.59)	1.0902	0.1442	0.1347	3641.5	2
B	4	3642.2	(3.15, 8.60, 5.06)	0.6949	0.2018	0.1792	3642	2
C	0.1	3641.8	(−8.55, 4.35, 5.12)	1.0912	0.1444	0.1346	3642	2
D	4.1	3642.8	(10.6, 1.16, 1.56)	0.6911	0.2022	0.1795	3642.5	2

calculated using Gaussian03[27] (see Table 1), and assume the same FWHM. For the four conformers the values are similar, $\sigma_{abs} = 2 \times 10^{-18}$ cm^2 (peak value), approx. three times the phenol value. Thus, σ_{abs} is approximately a factor 10^2 larger than the R-IRMPD cross section σ_{diss}. A simple interpretation of this ratio is that the molecule must absorb on the order of 10^2 photons in order to dissociate. Note that the corresponding total energy is approximately one order of magnitude larger than the UV dissociation energy (E_{diss} approx. 35 000 cm^{-1})[10]. Two effects may contribute to this factor. First, the excited molecule may fluoresce, either from the excited state, or from states that it evolves into as a consequence of IVR. In a very simple model, the ratio of decay rate Γ from the excited state *via* single or multiple photon emission and the total decay rate $A + \Gamma$, where A is the fluorescence rate, determines the actual energy deposition rate, $dE_{int}/dt = \sigma_{abs} I\Gamma/(\Gamma + A)$, where I is the intensity (stimulated emission is neglected). The ratio may be distinctively smaller than unity and contribute to a reduction of $\sigma_{diss} = (\Gamma/(A + \Gamma))(h\nu/E_{diss})\sigma_{abs}$. The fluorescence rate A for the excited vibrational state is calculated to be approximately 95 s^{-1}, using the transition dipole matrix elements given in Table 1. (The calculated stimulated emission rate at the OPO intensity shown in Fig. 12 (blue curves) is approximately 50 s^{-1}, smaller than A.) Second, the molecules, internally heated by energy deposition, will also "cool" by emission of black-body radiation.[28] Since the time scale over which dissociation is obtained under our experimental conditions is long (of order 1 s) this could be a process of relevance. Such a cooling process would also increase the number of IR photons necessary to be absorbed until sufficient energy is accumulated that leads to dissociation. A detailed explanation of the ratio $\sigma_{diss}/\sigma_{abs}$ is beyond the scope of this work, requiring extensive additional measurements.

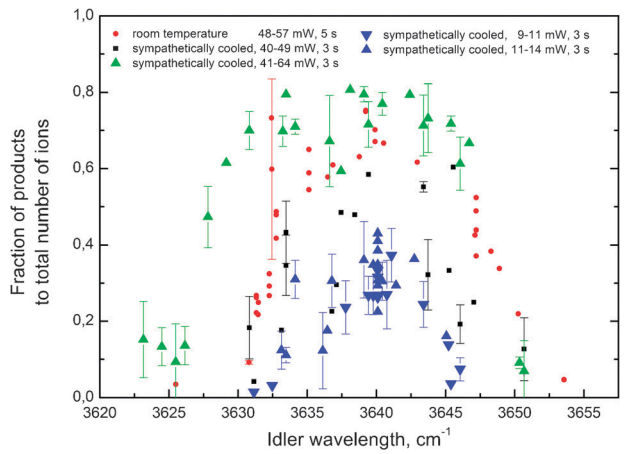

Fig. 12 Spectra of room-temperature (buffer-gas cooled) and laser-cooled photodestructed $HTyrAla^+$. The error of the room temperature (red) fraction of products is significantly larger than for the sympathetically cooled cases (green, black, blue). Total time to obtain the data shown here was about 2000 min.

The experimentally observed photodissociation spectra are shown in Fig. 12. It comprises data from several hundred individual measurements. The fundamental transition of the phenol-OH mode has the central wavelength of approx. 3640 cm^{-1}, within a few wavenumbers both for buffer-gas and sympathetically cooled ions. The measurements shown in blue are taken at the lowest intensities, and the maximum dissociation fraction is below 0.4. This implies that saturation effects are not important in this case. The full width of this line (for sympathetically cooled ions) is approx. 10 cm^{-1} and will be discussed in the following.

The measurements taken with buffer gas cooled molecules show a larger linewidth. This is likely due to both saturation (a larger OPO intensity was used) and to an increase of internal energy (rotational temperature) caused by partial transformation of micromotion energy, which is much larger for buffer-gas cooled ions than for sympathetically cooled ones, to internal energy during collisions with He atoms.

The observed transition linewidths contain information about the internal rotational temperature. However, this information cannot be extracted straightforwardly, as several unknowns contribute to it. First, the preparation step of our cold molecules is not sensitive to a conformer[10] having overall energies close or below the level $k_B \times$ (room temperature), so any ensemble of ions loaded into the trap is expected to contain various conformations and these will contribute to our spectroscopic signal. Different conformations have different rotational constants and vibrational transition frequencies (see Table 1). This introduces a broadening and shape change of the vibrational line. Second, in R-IRMPD, the molecule absorbs many photons before dissociating. The increasing internal energy may lead to an increasing distortion of the molecular structure. As this occurs, the vibrational frequency of the local mode may shift, yielding another cause of broadening. Third, the molecule may be heated rotationally. Fourth, the IVR process leads to line broadening of each ro-vibrational transition line in the band, washing out the fine structure of the rotational band.

The measurements by Stearns *et al.*[10] on $HTyrAla^+$ provide important information on these issues. In their work, vibrationally cold ions were obtained by collisions with cold He buffer gas atoms in a cryogenic trap. The vibrational temperature was measured to be 10–11 K and the rotational temperature was presumed to be in equilibrium. Their measurements include information on the relative shift of the vibrational lines for four conformers and also on the rotational band linewidths (see Section 1). It should be emphasized that their spectroscopic method was not R-IRMPD but vibrationally depleted electronic (UV) spectroscopy, in which only a single IR photon is absorbed, therefore a distortion-induced lineshift cannot contribute to their observed linewidths. As their work was focused on determining a wide IR spectrum rather than precisely measuring one particular line, a frequency step size of 0.5 cm^{-1} was sufficient. Their measurements indicate that the frequency shift between conformers is not more than about 1 cm^{-1} roughly consistent with the theoretical relative shifts. The FWHM linewidth of individual conformer species is about 1.7 cm^{-1}, after subtracting the contribution of the spectral linewidth of the pulsed OPO (linewidth *ca.* 1 cm^{-1}). Importantly, this linewidth includes the effect of IVR. Our 10 cm^{-1} linewidth (in the sympathetically cooled case) is substantially larger than both the "cryogenic" linewidth and the upper limit for the conformer shift. Therefore, in our sympathetically cooled case conformation variations and IVR broadening cannot be dominant effects. Instead, either our rotational temperature is significantly higher than 10 K or there is a substantial internal-energy-induced line shift, or both.

In order to discuss the influence of temperature on the band linewidth, simulations of the rotational band for different rotational temperatures were made. As input parameters the rotational constants as well as the vibrational transition dipole moments in the molecular frame, as computed by ref. 10 and reported in Table 1, were used. The rotational constants of the vibrational ground state are also used for the excited state, due to lack of any further information. The rotational band structure was computed using the program *PGOPHER*,[29] including transitions between rotational levels with quantum number up to $J = 510$. This high value was required in order to obtain a sufficiently complete band shape even at the highest considered temperature, $T = 1000$ K, at which a very large number of rotational levels in the ground state are thermally populated. The individual ro-vibrational transitions were broadened by a Lorentzian line shape function of 0.9 cm^{-1} full width at half maximum, in order to obtain a smooth band. A value smaller than the contributions from IVR and from the presence of more than one conformer(s) was chosen, in order not to smooth too much any thermal features. Fig. 13 shows the simulated spectra for different rotational temperatures. The resulting line shapes are not Gaussian. The simulated spectrum for 10 K (where a reduced broadening of 0.067 cm^{-1} has been used in order to show the structure of the band more clearly) has a width of 1 cm^{-1}, which can be compared with the measurements of ref. 10 (approx. 1.7 cm^{-1}). The simulated width is smaller, but an additional contribution coming from IVR broadening must be considered as well. Yamada *et al.*[30,31] have measured the lifetime of the upper vibrational state of the OH vibration in phenol as 14 ps,

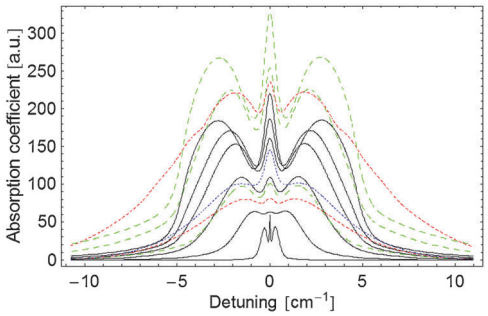

Fig. 13 Simulated rotational bands of the phenol OH vibration of $HTyrAla^+$. Full lines: conformer A. The temperatures are, increasing from the smallest line, 10 K, 100 K, 300 K, 450 K, 600 K, 1000 K. The red/medium-long-dashed (green/long-dashed, blue/short-dashed) lines are for the B (C, D) conformer. The FWHMs are as follows. Conformer A: 1 cm^{-1} (10 K), 3.9 cm^{-1} (100 K), 6.2 cm^{-1} (300 K), 7.3 cm^{-1} (450 K), 8.1 cm^{-1} (600 K), 9.2 cm^{-1} (1000 K); conformer B: 8.5 cm^{-1} (300 K), 11 cm^{-1} (600 K); conformer C: 6.5 cm^{-1} (300 K), 8.4 cm^{-1} (600 K), 9.2 cm^{-1} (1000 K); conformer D: 6.5 cm^{-1} (300 K). The vertical scale is arbitrary for all curves, also for different temperatures of a single conformer.

which corresponds to a linewidth of 0.4 cm^{-1}. It is conceivable that the lifetime is shorter in HTyrAla, due to its larger density of states as compared to that of phenol, which may provide more doorway states. The IVR rate strongly depends on such states, as has been shown by Yamada *et al.*, who found, *e.g.* a six times smaller rate when the phenol ring is deuterated (phenol-d_5), which significantly changes the vibrational frequencies of the molecule, and a three times higher rate in the case of the OH vibration. Such effects may explain the slightly larger linewidth value observed by Stearns *et al.*

For rotational temperatures from room temperature on, the simulated linewidths increase only slowly with temperature, *e.g.* at $T = 100$, 300, 450, 600, 1000 K the simulated FWHMs are approximately 3.9, 6.2, 7.3, 8.1, 9.2 cm^{-1} for conformer A. Thus, in principle the FWHM can be correlated with rotational temperature, but obtaining a high temperature resolution would require an accurate measurement of the bandshape. This was not possible in our work, due to variations in the ion flux and the limited signal-to-noise ratio achieved with the low trapped ion number. For comparison, conformers B, C, D were also simulated, which have linewidths 8.5, 6.5, 6.5 cm^{-1} at 300 K, respectively. Conformer B has a significantly larger FWHM at room temperature and above than conformers A and C. This variability further makes an accurate determination of rotational temperature difficult in the case of a mixture of conformers. The observed FWHM of 10 cm^{-1} corresponds to an effective rotational temperature in the range from above 600 K to above but near 1000 K, significantly above 300 K that the molecules are expected to have after collisions with 300 K helium buffer gas.

7 Conclusion

Vibrational spectroscopy of a local mode of a sympathetically cooled polyatomic molecular ion was demonstrated, for the first time to our knowledge. The vibrational excitation of polyatomic $HTyrAla^+$ ions was induced by irradiation with

continuous-wave infrared light at 2.74 μm and led to photodissociation *via* the R-IRMPD process. For comparison, experiments were also performed on uncooled ions. The kinetic energy of the ions was significantly different in these two cases. After loading of the ions into the trap, room-temperature He gas was introduced as a first translational cooling step. In the case of subsequent sympathetic cooling, the rotational temperature may be assumed to have reached a value on the order of 300 K, since interaction with the 300 K black-body radiation is dominant. Without sympathetic cooling, the ion micromotion energy may have been partially converted to internal energy, leading to an increased rotational temperature.

For the lower IR intensities used, a photodissociation rate was observed that is linearly dependent on intensity, and allowed determination of the approximate R-IRMPD cross section. It is significantly (approx. two orders) lower than the vibrational absorption cross section, indicating that a significantly larger number of IR photons must be absorbed before dissociation can take place, than that corresponding to a typical bond energy. The R-IRMPD spectral lines exhibited modest signal-to-noise ratios, limited by the fact that the individual dissociation experiments are performed with small number of ions and this number fluctuates from one loading to the next. By comparison with measurements by Stearns and coworkers on $HTyrAla^+$ cooled by cold He buffer gas, we deduce that the observed linewidth of the vibrational transition (10 cm^{-1}) is not dominated by IVR from the upper vibrational state, nor by the small frequency shifts among conformers that are present as a mixture in our molecular samples. Instead, it is due to a combination of rotational temperature imposed by the initial preparation, the interaction with black-body radiation of the environment, a possible increase of rotational temperature in the course of absorbing the approx. 80 IR photons, and a shift of the vibrational frequency with increasing internal energy in the molecule. The latter would be caused by cross-coupling anharmonicities of the molecule's modes (and is probably a dominant effect). Phenomenologically, the effective temperature to be assigned to the line is significantly above room temperature, approximately 1000 K. Further studies (experimental and *ab initio* calculations) should allow disentangling the mentioned effects.

Future investigations could be aimed at (i) an accurate determination of the IVR-induced broadening, by performing measurements as in ref. 10, but using an injection-seeded pulsed OPO with reduced linewidth, (ii) determining more precisely the influence of internal-energy-induced broadening, by performing R-IRMPD on rotationally cold $HTyrAla^+$ in a cryogenic trap apparatus as used by Stearns *et al.* in order to reduce the effects of high rotational temperature on the spectral line shape, and measuring with high signal-to-noise ratio the rotational band shape. As for (i), the measurements should be performed on samples containing a single conformer, which can be obtained by selectively UV-dissociating other conformers. Moreover, a combination IR-multiphoton absorption and IR-depletion spectroscopy could be applied: the vibrational lineshape is measured by IR-depletion spectroscopy using an injection-seeded pulsed OPO with reduced linewidth, but preceding the interrogation by multi-photon IR excitation for a fixed but variable time, under conditions that the molecules mostly remain undissociated. In this way, one could determine the line shift as a function of internal energy. One could also measure the vibrational temperature as a function of internal energy, using hot band intensities as indicators. In such measurements, the cryogenic buffer gas should first be removed from the trap in order not to continue rotational cooling. Under such conditions, the molecules would still be rotationally and vibrationally cooled by IR emission, but with a reduced rate. A determination of this cooling rate is itself an interesting aim.

Acknowledgements

The authors are grateful to H. Gollnick for collaboration on the experiment, to T. Schneider for helpful discussions and to B. Roth for his contributions in the initial phase of this project. We especially acknowledge T. Rizzo, J. Stearns, and T. Wassermann for important suggestions, discussions and communication of unpublished results. This work was funded by the DFG under grant SCHI 431/12-1.

References

1 T. Schneider, B. Roth, H. Duncker, I. Ernsting and S. Schiller, All-optical preparation of molecular ions in the rovibrational ground state, *Nat. Phys.*, 2010, **6**, 275–278.
2 P. Staanum, K. Højbjerre, P. Skyt, A. Hansen and M. Drewsen, Rotational laser cooling of vibrationally and translationally cold molecular ions, *Nat. Phys.*, 2010, **6**, 271–274.
3 I. Vogelius, L. Madsen and M. Drewsen, Blackbody-Radiation-Assisted Laser Cooling of Molecular Ions, *Phys. Rev. Lett.*, 2002, **89**, 173003.
4 S. Nielsen, J. Andersen, P. Hvelplund, L. Liu and S. Tomita, Biomolecular ions in accelerators and storage rings, *J. Phys. B: At., Mol. Opt. Phys.*, 2004, **37**, 25–56.
5 B. Roth, J. Koelemeij, H. Daerr and S. Schiller, Rovibrational spectroscopy of trapped molecular hydrogen ions at millikelvin temperatures, *Phys. Rev. A: At., Mol., Opt. Phys.*, 2006, **74**, 040501–040504.
6 J. Koelemeij, B. Roth, A. Wicht, I. Ernsting and S. Schiller, Vibrational Spectroscopy of HD^+ with 2 ppb Accuracy, *Phys. Rev. Lett.*, 2007, **98**, 173002–173004.
7 U. Bressel, *et al.*, Heinrich-Heine-Universität Düsseldorf, priv. communication.
8 C. Correia, C. Clavaguera, U. Erlekam, D. Scuderi and G. Ohanessian, IRMPD spectroscopy of a protonated, phosphorylated dipeptide, *ChemPhysChem*, 2008, **9**, 2564–2573.
9 T. Dienes, S. Pastor, S. Schürch, J. Scott, J. Yao, S. Cui and C. Wilkins, Fourier transform mass spectrometry—advancing years (1992–mid. 1996), *Mass Spectrom. Rev.*, 1996, **15**, 163–211.
10 J. Stearns, M. Guidi, O. Boyarkin and T. Rizzo, Conformation-specific infrared and ultraviolet spectroscopy of tyrosine-based protonated dipeptides, *J. Chem. Phys.*, 2007, **127**, 154322–154327, and private communication.
11 G. Gregoire, M. P. Gaigeot, D. C. Marinica, J. Lemaire, J. P. Schermann and C. Desfrançois, Resonant infrared multi-photon dissociation spectroscopy of gas-phase protonated peptides. Experiments and Car–Parrinello dynamics at 300 K, *Phys. Chem. Chem. Phys.*, 2007, **9**, 3082–3097.
12 J. Black, P. Kolodner, M. Shultz, E. Yablonovitch and N. Bloembergen, Collisionless multiphoton energy deposition and dissociation of SF_6, *Phys. Rev. A: At., Mol., Opt. Phys.*, 1979, **19**, 704–716.
13 N. Polfer and J. Oomens, Vibrational spectroscopy of bare and solvated ionic complexes of biological relevance, *Mass Spectrom. Rev.*, 2009, **28**, 468–494.

14 J. Oomens, B. Sartakov, G. Meijer and G. von Helden, Gas-phase infrared multiple photon dissociation spectroscopy of mass-selected molecular ions, *Int. J. Mass Spectrom.*, 2006, **254**, 1–19.
15 N. Barnes, S. Benson, F. Duarte, C. Freed, D. Harris, R. Sze and P. Zorabedian, *Tunable Lasers Handbook*, Academic, 1995.
16 S. Vasilyev, H. Gollnick, A. Nevsky, A. Grisard, E. Lallier, B. Gerard, J. Jimenez and S. Schiller, Counterdirectional mode coupling in ring resonators with QPM nonlinear crystals and effects on the characteristics of cw optical parametric oscillation, *Appl. Phys. B: Lasers Opt.*, 2010, **100**, 737–747.
17 A. Ostendorf, C. Zhang, M. Wilson, D. Offenberg, B. Roth and S. Schiller, Sympathetic Cooling of Complex Molecular Ions to Millikelvin Temperatures, *Phys. Rev. Lett.*, 2006, **97**, 243005.
18 A. Ostendorf, *Sympathetische Kühlung von Molekülionen durch lasergekühlte Bariumionenin einer linearen Paulfalle*, *PhD dissertation*, Heinrich-Heine-Universität Düsseldorf, 2006 (http://docserv.uni-duesseldorf.de/servlets/DocumentServlet?id = 3404).
19 D. Offenberg, *Studies of trapped, cooled ion ensembles*, *PhD dissertation*, Heinrich-Heine-Universität Düsseldorf, 2009 (http://docserv.uni-duesseldorf.de/servlets/DocumentServlet?id = 13566).
20 D. Offenberg, C. Zhang, Ch. Wellers, B. Roth and S. Schiller, Translational cooling and storage of protonated proteins in an ion trap at subkelvin temperatures, *Phys. Rev. A: At., Mol., Opt. Phys.*, 2008, **78**, 061401.
21 C. B. Zhang, *Production and sympathetic cooling of complex molecular ions*, *PhD Dissertation*, Heinrich-Heine-Universität Düsseldorf, 2008 (http://docserv.uni-duesseldorf.de/servlets/DocumentServlet?id = 9606).
22 L. Hornekær, *Single- and multi-species Coulomb ion crystals: Structures, dynamics and sympathetic cooling*, *PhD dissertation*, University of Århus, 2000.
23 M. Drewsen and A. Brøner, Harmonic linear Paul trap: Stability diagram and effective potentials, *Phys. Rev. A: At., Mol., Opt. Phys.*, 2000, **62**, 045401.
24 B. Roth, A. Ostendorf, H. Wenz and S. Schiller, Production of large molecular ion crystals *via* sympathetic cooling by laser-cooled Ba^+, *J. Phys. B: At., Mol. Opt. Phys.*, 2005, **38**, 3673–3685.
25 D. Berkeland, J. Miller, J. Bergquist, W. Itano and D. Wineland, Minimization of ion micromotion in a Paul trap, *J. Appl. Phys.*, 1998, **83**, 5025–5033.
26 S. Ishiuchi, M. Fujii, T. Robinson, B. Miller and H. Kjaergaard, Vibrational overtone spectroscopy of phenol and its deuterated isotopomers, *J. Phys. Chem. A*, 2006, **110**, 7345–7354.
27 M. J. Frisch, G. W. Trucks, H. B. Schlegel, G. E. Scuseria, M. A. Robb, J. R. Cheeseman, J. A. Montgomery, Jr., T. Vreven, K. N. Kudin, J. C. Burant, J. M. Millam, S. S. Iyengar, J. Tomasi, V. Barone, B. Mennucci, M. Cossi, G. Scalmani, N. Rega, G. A. Petersson, H. Nakatsuji, M. Hada, M. Ehara, K. Toyota, R. Fukuda, J. Hasegawa, M. Ishida, T. Nakajima, Y. Honda, O. Kitao, H. Nakai, M. Klene, X. Li, J. E. Knox, H. P. Hratchian, J. B. Cross, V. Bakken, C. Adamo, J. Jaramillo, R. Gomperts, R. E. Stratmann, O. Yazyev, A. J. Austin, R. Cammi, C. Pomelli, J. W. Ochterski, P. Y. Ayala, K. Morokuma, G. A. Voth, P. Salvador, J. J. Dannenberg, V. G. Zakrzewski, S. Dapprich, A. D. Daniels, M. C. Strain, O. Farkas, D. K. Malick, A. D. Rabuck, K. Raghavachari, J. B. Foresman, J. V. Ortiz, Q. Cui, A. G. Baboul, S. Clifford, J. Cioslowski, B. B. Stefanov, G. Liu, A. Liashenko, P. Piskorz, I. Komaromi, R. L. Martin, D. J. Fox, T. Keith, M. A. Al-Laham, C. Y. Peng, A. Nanayakkara, M. Challacombe, P. M. W. Gill, B. Johnson, W. Chen, M. W. Wong, C. Gonzalez and J. A. Pople, *GAUSSIAN 03 (Revision C.02)*, Gaussian, Inc., Wallingford CT, 2004.
28 R. Dunbar, Infrared radiative cooling of gas-phase ions, *Mass Spectrom. Rev.*, 1992, **11**, 309–339.
29 C. M. Western, , *PGOPHER, a Program for Simulating Rotational Structure*, University of Bristol, http://pgopher.chm.bris.ac.uk, retrieved May 9, 2011. We used the parameter *Intensity Units* = Arbitrary.
30 Y. Yamada, T. Ebata, M. Kayano and N. Mikami, Picosecond IR–UV pump–probe spectroscopic study of the dynamics of the vibrational relaxation of jet-cooled phenol. I. Intramolecular vibrational energy redistribution of the OH and CH stretching vibrations of bare phenol, *J. Chem. Phys.*, 2004, **120**, 7400.
31 Y. Yamada, Y. Katsumoto and T. Ebata, Picosecond IR-UV pump–probe spectroscopic study on the vibrational energy flow in isolated molecules and clusters, *Phys. Chem. Chem. Phys.*, 2007, **9**, 1170–1185.
32 I. Compagnon, J. Oomens, G. Meijer and G. von Helden, Mid-Infrared Spectroscopy of Protected Peptides in the Gas Phase: A Probe of the Backbone Conformation, *J. Am. Chem. Soc.*, 2006, **128**(11), 3592–3597.